RSC Advances

PAPER

View Article Online
View Journal | View Issue

Cite this: *RSC Adv.*, 2021, **11**, 34137

Self-supported Cu_3P nanowire electrode as an efficient electrocatalyst for the oxygen evolution reaction†

Xin Zhou,[a] Xiaoliang Zhou,*[a] Limin Liu,*[a] Hanyu Chen,[a] Xingguo Hu,[a] Jiaqi Qian,[a] Di Huang,[a] Bo Zhang[b] and Junlei Tang*[a]

Hydrogen is an ideal energy carrier due to its abundant reserves and high energy density. Electrolyzing water is one of the carbon free technologies for hydrogen production, which is limited by the sluggish kinetics of the half reaction of the anode – the oxygen evolution reaction (OER). In this study, a self-supported Cu_3P nanowire (Cu_3P NWs/CF) electrode is prepared by electrodeposition of a $Cu(OH)_2$ nanowire precursor on conductive Cu foam ($Cu(OH)_2$ NWs/CF) with a subsequent phosphating procedure under a N_2 atmosphere. When used as an OER working electrode in 1.0 M KOH solution at room temperature, Cu_3P NWs/CF exhibits excellent catalytic performance with an overpotential of 327 mV that delivers a current density of 20 mA cm^{-2}. Notably, it can run stably for 22 h at a current density of 20 mA cm^{-2} without obvious performance degradation. This highly efficient and stable OER catalytic performance is mainly attributed to the unique nanostructure and stable electrode construction. Interestingly, this synthesis strategy has been proved to be feasible to prepare large-area working electrodes (*e.g.* 40 cm^{-2}) with unique nanowire structure. Therefore, this work has provided a good paradigm for the mass fabrication of self-supporting non-noble metal OER catalysts and effectively promoted the reaction kinetics of the anode of the electrolyzing water reaction.

Received 19th July 2021
Accepted 10th October 2021

DOI: 10.1039/d1ra05526g

rsc.li/rsc-advances

Introduction

Increasing attention to new energy and environmental issues has promoted extensive research on energy storage and conversion technologies.[1,2] Water splitting driven by electricity has been considered to be a promising method to generate sustainable hydrogen.[3,4] The oxygen evolution reaction (OER) is the anode half reaction of the electrochemical water splitting reaction, which is a slow kinetic process involving four electron–proton transfer and coupling.[5–7] Therefore, OER is critical to the overall energy consumption and efficiency of the electrolyzing water reaction, thus designing OER electrocatalysts with high catalytic activity and stability is highly required. Recent studies have shown that noble metal based catalysts (such as RuO_2 and IrO_2) have good electrocatalytic activity for OER.[8–10] However, their large-scale application is greatly compromised by their low reserves and high cost. Therefore, it is highly imperative to explore non-precious metal based OER electrocatalysts with high catalytic activity and stability.

Recently, transition metal phosphides (TMPs) have attracted great interest in electrocatalytic OER owing to the low cost, good electrical conductivity, and high catalytic activity.[11–13] Many kinds of TMPs, such as Co_2P,[14] CoP,[15] Ni_2P,[16] and Fe_2P[17] were synthesized and proved to be excellent and durable OER electrocatalysts. However, most of these catalysts are powder catalysts and cannot be used directly as OER working electrode, which need to be coated on current collector with the aid of binder. The binder will cover part of electrocatalytic active sites and not conducive to the stability of the working electrode.[18] Recently, the electrocatalysts with unique nanostructures grown directly on various conductive substrates have been proved to be a promising strategy for improving the catalytic activity and stability for OER working electrode.[19,20] For example, Qiao and co-workers reported the preparation of Co_3O_4–carbon porous nanowire arrays on Cu foil by oxidizing a Co-based metal organic framework and used as an electrocatalyst for OER, which can generate a stable current density of 10.0 mA cm^{-2} with an overpotential of 290 mV in alkaline electrolyte.[21] Jiang and co-workers reported the synthesis of CoP films on Cu foil *via* an electrodeposition method, which can achieved a current density of 10 mA cm^{-2} with an overpotential of 345 mV in alkaline media.[22] However, previous studies have mainly focused on the preparation of small area membrane catalysts in the laboratory, such as usually less than 5 cm^{-2}. For a water splitting device, a large-area of working electrode with efficient,

[a]*College of Chemistry and Chemical Engineering, Southwest Petroleum University, Chengdu, 610500, PR China. E-mail: xlzhou_swpu@sina.com*

[b]*Hydrogen Energy Division, Dong Fang Boiler Group Co., Ltd., Chengdu, 611731, PR China*

† Electronic supplementary information (ESI) available. See DOI: 10.1039/d1ra05526g

inexpensive, and stable catalysts is highly required.[23] Compared with other transition metals based catalysts such as Fe, Co, and Ni, Cu based catalysts have more advantages in price and reserves. Although the OER activity of Cu based catalysts is lower than that of other transition metal based catalysts, it can still be used as a substitute for noble metal catalysts.[24,25] Although Cu_3P has been reported as OER catalysts with excellent catalytic activity in alkaline electrolyte, the preparation of large-area Cu_3P on Cu foam substrate has not been reported.[26,27]

In this regard, we had prepared Cu_3P nanowires on Cu foam *via* a simple two-step method. Firstly, $Cu(OH)_2$ NWs/CF was obtained through *in situ* electrochemical anodic oxidation, in which the Cu foam served as both current collector and copper source. And then $Cu(OH)_2$ NWs/CF was converted to Cu_3P/NWs after a phosphating process. The as-prepared Cu_3P NWs/CF electrode exhibited high-efficient activities and outstanding stabilities for OER in alkaline media due to the unique nanostructure and the high conductivity of Cu foam. Notably, this simple two-step method has been proved to be suitable for the preparation of large-area Cu_3P electrode (such as 40 cm^{-2}), which provides a universal method for the mass fabrication of OER electrodes with high performance.

Experimental

Materials and instrumentation

All chemical reagents used in this study were all analytical graded and utilized directly without any further purification. Cu foam was purchased from Hefei Kejing Material Technology Co., Ltd. Powder X-ray diffraction (XRD) patterns were collected on a RIGAKU Ultima IV, and X-ray diffractometer was attained by Cu-Kα radiation at a scanning rate of 2° min^{-1}. Field-emission scanning electron microscopy (FESEM) measurements were performed on Carl Zeiss Supra-55. Transmission electron microscope (TEM) measurements were conducted on FEI Talos F200s, operating at 200 kV. XPS was carried out on ESCALAB 250 instrument to determine chemical-state of the samples.

Synthesis of $Cu(OH)_2$ nanowires on Cu foam (labelled as $Cu(OH)_2$ NWs/CF)

Firstly, a piece of Cu foam (1 cm × 2 cm) was cleaned by ultrasonication in 2 M HCl aqueous solution, ethanol, and deionized water for 5 minutes, respectively. This process is used to remove the surface oxide layer in the Cu foam. $Cu(OH)_2$ NWs/CF was prepared by electrochemical anodic oxidation method (0.02 A cm^{-2} for 600 s) using a two-electrode system with Ti sheet as the counter electrode and Cu foam as the working electrode. Then, the as-prepared $Cu(OH)_2$ NWs/CF was dried in a vacuum oven at 60 °C overnight.

Synthesis of Cu_3P nanowires on Cu foam (labelled as Cu_3P NWs/CF)

Cu_3P NWs/CF was prepared by low-temperature phosphorization of $Cu(OH)_2$ NWs/CF. Specifically, the $NaH_2PO_2 \cdot H_2O$ and obtained $Cu(OH)_2$ NWs/CF precursor were put into two different ceramic boats, and then the ceramic boat with $NaH_2PO_2 \cdot H_2O$ was placed on the upstream side and the ceramic boat with $Cu(OH)_2$ NWs/CF precursor was placed at the center of tube furnace. After evacuating the air out of the tube furnace for 30 min, the samples were heated at 270 °C for 2 h at a heating rate of 2 °C min^{-1} under N_2 atmosphere.

For comparison, a pice of bare Cu foam (1 cm × 2 cm) was phosphated using the identical procedure, the as-prepared samples were labeled as Cu_3P/CF in this paper.

Synthesis of RuO_2 on Cu foam (labeled as RuO_2/CF)

The RuO_2/CF was prepared as follows: 5 mg of RuO_2 was dispersed into a mixture containing 600 μL of ethanol, 340 μL of water, and 60 μL of Nafion solution (5 wt%). The solution was sonicated for 45 min to generate a homogeneous ink. Then, 100 μL of the homogeneous ink was dropped onto Cu foam (1 cm × 0.5 cm) and dried overnight at ambient conditions.

Electrochemical measurements

All electrochemical tests were performed using the three-electrode system in CHI 660E electrochemical workstation. The as-prepared samples on Cu foam, Pt sheet, and Ag/AgCl were used as the working electrode, the counter electrode, and reference electrode, respectively. The linear sweep voltammetry (LSV) curves were recorded in 1.0 M KOH solution at a scan rate of 2 mV s^{-1} after several cyclic voltammetry (CV) cycles at a sweep rate of 100 mV s^{-1}. The potentials were calibrated relative to hydrogen electrode (ERHE) based on the equation: $E_{RHE} = 0.197 + 0.059 \times pH + E_{Ag/AgCl}$. Electrochemical impedance spectroscopy (EIS) was measured at 1.6 V *versus* RHE in the frequency range from 100 kHz to 0.01 Hz. Chronoamperometric response (*i*–*t*) tests were evaluated to certify the stability. CV curves at different scan rates (20, 40, 60, 80, 100, and 120 mV s^{-1}) were performed in non-faradaic potential range from 0.9 to 1.0 V (*vs.* RHE) to probe the electrochemical double-layer capacitance (C_{dl}).

Results and discussion

Cu foam has a large surface area, porous structure, and excellent stability and conductivity under alkaline conditions, which is beneficial to promote the OER reaction.[28,29] The Cu_3P nanowires on Cu foam (Cu_3P NWs/CF) was synthesized by a simple two-step method, as shown in Fig. 1. The $Cu(OH)_2$ nanowires precursor ($Cu(OH)_2$ NWs/CF) was first obtained by electrochemical anodic oxidation on Cu foam in 1.0 M KOH solution. Powder X-ray diffraction (XRD) patterns of $Cu(OH)_2$ NWs/CF (Fig. S1†) shows that the diffraction peaks at 16.8°, 23.8°, 33.9°, 35.7°, 38.0°, and 39.5° matched well with the (020), (021), (002), (111), (022), and (130) facets of $Cu(OH)_2$ (PDF # 80-0656), indicating that the successful preparation of $Cu(OH)_2$ on Cu foam. Besides, the three strong peaks at 43.1°, 50.3°, and 74.0° are attributed to the (111), (200), and (220) facets of Cu (Fig. S2†). Further, the final product of Cu_3P NWs/CF was obtained by phosphating the $Cu(OH)_2$ NWs/CF with $NaH_2PO_2 \cdot H_2O$ as the P source under N_2 atmosphere. The colour of Cu

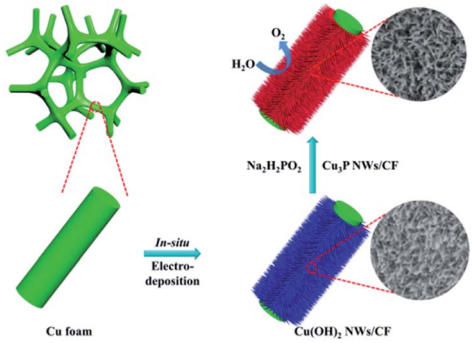

Fig. 1 Schematic illustration of the formation of Cu_3P NWs/CF.

foam changed from saffron yellow to blue, which eventually became black after low temperature phosphating at 270 °C (Fig. S3†).

The morphology of $Cu(OH)_2$ NWs/CF and Cu_3P NWs/CF were observed by scanning electron microscopy (SEM). The low-magnification SEM image of $Cu(OH)_2$ NWs/CF (Fig. 2a) shows that uniform and dense $Cu(OH)_2$ nanowires were grown on the surface of Cu foam. From the corresponding high-magnification SEM images, $Cu(OH)_2$ nanowires exhibited a smooth surface (Fig. 2b and c). For comparison, the SEM images of bare Cu foam are also shown in Fig. S4.† The SEM images of the Cu_3P NWs/CF are shown in Fig. 2d–f. After phosphating with $NaH_2PO_2 \cdot H_2O$ at 270 °C under N_2 atmosphere, the as-prepared Cu_3P NWs/CF samples can inherit the morphology of $Cu(OH)_2$ nanowires precursors. The dense Cu_3P nanowires uniformly covered the Cu foam surface as shown in Fig. 2d. Compared with $Cu(OH)_2$ NWs/CF, Cu_3P NWs/CF samples exhibited a much rough surface (Fig. 2e and f). The scanning electron microscopy energy dispersive X-ray spectroscopy (SEM-EDX) elemental mapping images showed that Cu and P elements are uniformly distributed in Cu_3P NWs/CF (Fig. S5†). For comparison, the bare Cu foam was also phosphated *via* a similar procedure (labelled as Cu_3P/CF). The results show that Cu_3P obtained by directly phosphating Cu foam does not have a unique nanostructure (Fig. S6 and S7†).

The morphology of the as-prepared $Cu(OH)_2$ and Cu_3P nanowires were further investigated by transmission electron microscopy (TEM). Fig. 3a and b displays the TEM images of $Cu(OH)_2$ and Cu_3P nanowires, suggesting the smooth surface of

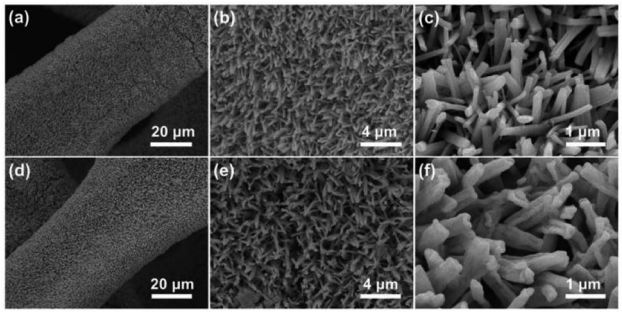

Fig. 2 SEM images of (a–c) $Cu(OH)_2$ NWs/CF and (d–f) Cu_3P NWs/CF.

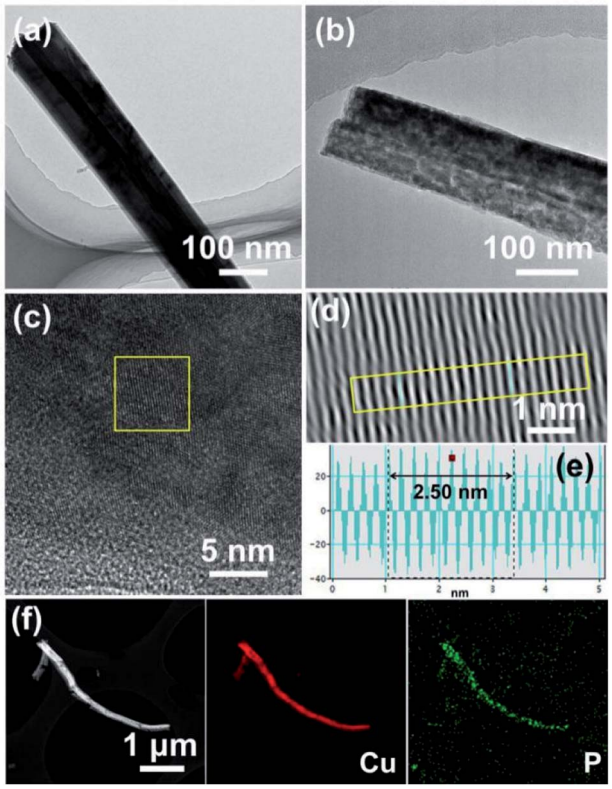

Fig. 3 (a) TEM image of $Cu(OH)_2$ NWs/CF, (b) TEM image of Cu_3P NWs/CF, (c) HRTEM image of Cu_3P NWs/CF, (d) the inverse fast Fourier transformation (IFFT) image of the rectangular region in figure (c), (e) the corresponding line scan of the rectangular region in figure (d), and (f) the elemental mapping images of Cu and P of Cu_3P NWs/CF.

$Cu(OH)_2$ nanowires became rough and porous after phosphorization. This unique morphology can not only promote the contact between electrolyte and catalyst, but also enhance the release of oxygen bubbles, leading to the enhancement of OER catalytic activity.[30–33] The high-resolution TEM (HRTEM) image and the inverse fast Fourier transformation (IFFT) image of Cu_3P NWs/CF exhibit that an inter-planar spacing of 0.25 nm, which is assigned to the (112) plane of Cu_3P (Fig. 3c–e). The scanning TEM (STEM) image and the corresponding EDX elemental mapping images of P and Cu in Cu_3P NWs/CF are shown in Fig. 3f, indicating that Cu and P elements are uniformly distributed in the whole nanowire. These results confirmed the successful synthesis of Cu_3P NWs/CF on Cu foam.

The XRD patterns of Cu_3P NWs/CF shows that the diffraction peaks at 36.2°, 39.3°, 41.8°, 45.1°, 46.5°, and 47.3° are indexed as the (112), (202), (211), (300), (113), and (212) planes of Cu_3P (PDF # 02-1263) (Fig. 4a). In addition, the diffraction peaks at 43.3°, 50.4°, and 74.1° were attributed to (111), (200), and (220) planes of Cu. XRD measurement results show that the successful formation of Cu_3P. X-ray photoelectron spectroscopy (XPS) spectrum was conducted to investigate the surface chemical composition and element valence states of the Cu_3P NWs/CF. The survey scan spectrum in Fig. 4b shows the presence of Cu, P, C, and O elements, while the presence of O element may be caused by carbon contamination and air

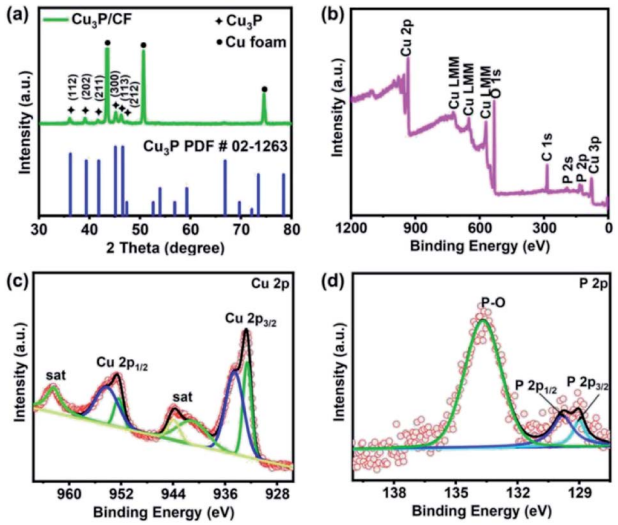

Fig. 4 (a) XRD patterns of Cu_3P NWs/CF, (b) XPS survey spectrum of Cu_3P NWs/CF, high-resolution XPS spectra of (c) Cu 2p and (d) P 2p for Cu_3P NWs/CF.

exposure.[34–36] Fig. 4c shows the high-resolution XPS spectrum of Cu 2p. The peaks at 932.6 and 952.2 eV are corresponded to the $Cu^{\delta+}$ $2p_{3/2}$ and $Cu^{\delta+}$ $2p_{1/2}$ (δ is likely close to 0) in Cu_3P, while the peaks at 934.6 and 954.7 eV are corresponding to the oxidized Cu^{2+} $2p_{3/2}$ and Cu^{2+} $2p_{1/2}$. The peaks at 941.1 eV, 943.9 eV, and 962.4 eV are attributed to the satellite peaks.[37,38] Fig. 4d shows that the peaks of P 2p are located at 129.1 eV and 129.9, corresponding to the P $2p_{3/2}$ and P $2p_{1/2}$, respectively, which are the characteristic peaks of P in Cu_3P.[38,39] In addition, the peak located at 132.7 eV can be assigned to P–O bonds, which probably due to the surface oxidation of Cu_3P after being exposure to air.[40,41]

The electrocatalytic activity of Cu_3P NWs/CF toward OER was investigated by a typical three-electrode system in an alkaline solution of 1.0 M KOH. For comparison, the reference samples, including Cu_3P/CF, commercial RuO_2/CF, and bare Cu foam were also measured in this study. In order to provide reliable electrochemical data and eliminate the effects of oxidative peaks, linear sweep voltammetry (LSV) curves of various samples were recorded from high potential to low potential with a 2 mV s^{-1} scan rate.[25,41] As shown in Fig. 5a and S13,† the Cu_3P NWs/CF electrode displayed an excellent OER catalytic performance with a low overpotential of 327 mV to reach a current density of 20 mA cm^{-2}, which is much lower than the RuO_2/CF (370 mV), Cu_3P/CF (386 mV), and Cu foam (427 mV). Moreover, at a current density of 50 mA cm^{-2}, the overpotential of Cu_3P NWs/CF (352 mV) is much smaller than those of RuO_2/CF (409 mV), Cu_3P/CF (459 mV), and Cu foam (500 mV). To investigate the effect of Pt as counter electrode on OER activity, a graphite rod was used as counter electrode to measure LSV curve under the same conditions (Fig. S12†). The results show that LSV curve has no obvious change, indicating that Pt has a negligible effect on OER performance.[42] These results suggest that the Cu_3P NWs/CF can promote the OER in alkaline electrolyte. We also summarize that the OER performance of other OER

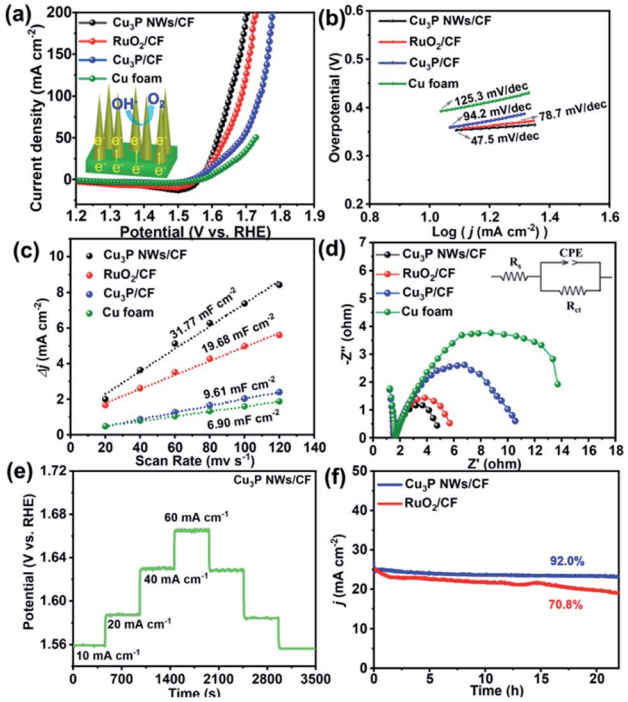

Fig. 5 (a) LSV curves (inset is the schematic diagram of electron transport on Cu_3P NWs/CF), (b) Tafel plots, (c) Capacitive currents as a function of scan rates, and (d) Nyquist plots (inset is the fitted equivalent circuit) of various samples. (e) Multi-current steps chronopotentiometry curve of Cu_3P NWs/CF. (f) Long-term stability of Cu_3P NWs/CF and RuO_2/CF at 20 mA cm^{-2}.

electrocatalysts in previous reported articles (Table S1†). The OER performance of Cu_3P NWs/CF electrode is comparable or much better than other previous reported electrocatalysts.

Furthermore, the Tafel slopes for all catalysts were investigated to have an insight into the OER kinetics of the working electrode.[43,44] The Tafel slope of Cu_3P NWs/CF is 74.5 mV dec^{-1}, which is lower than those of RuO_2/CF (78.7 mV dec^{-1}), Cu_3P/CF (94.2 mV dec^{-1}), and CF (125.3 mV dec^{-1}), implying a favorable OER kinetics for Cu_3P NWs/CF (Fig. 5b). The double-layer capacitances (C_{dl}) were obtained based on CV curves against various scan rates (20, 40, 60 80 100, and 120 mV s^{-1}) (Fig. S8†).[45,46] The Cu_3P NWs/CF shows the larger C_{dl} value of 31.77 mF cm^{-2} than those of RuO_2/CF (19.68 mF cm^{-2}), Cu_3P/CF (9.61 mF cm^{-2}), and CF (6.90 mF cm^{-2}) (Fig. 5c), which indicates that Cu_3P NWs/CF has more electrocatalytic active sites. Electrochemical impedance spectrum (EIS) was conducted to explore the electrode kinetics.[47,48] As depicted in Fig. 5d and Table S2,† Cu_3P NWs/CF has a much smaller charge-transfer resistance (3.6 ohm) than RuO_2/CF (4.5 ohm), Cu_3P/CF (9.5 ohm), and Cu foam (14.4 ohm), implying a fast charge transfer process of Cu_3P NWs/CF. The present Cu_3P NWs/CF sample was firmly anchored to the Cu foam, which can effectively reduce the interface gap between the catalyst and substrate, promoting the mass and charge transfer (inset to Fig. 1a). Fig. 5e shows that the each step of multi-step chronopotentiometry curve remained unchanged for as long as 500 s with the current density of 10 mA cm^{-2}, 20 mA cm^{-2}, 40 mA cm^{-2} and 60 mA cm^{-2}, indicating an

excellent mechanical robustness and mass transportation of Cu_3P NWs/CF towards OER.[49,50]

The long-term durability of Cu_3P NWs/CF and RuO_2/CF were employed by chronoamperometric in 1.0 M KOH (Fig. 5f). The Cu_3P NWs/CF exhibited 92% of the initial current density after 22 h sustained reaction, while RuO_2/CF just showed 70.8% of the initial current density, suggesting high stability of the Cu_3P NWs/CF. Meanwhile, LSV curves of Cu_3P NWs/CF showed that there was no significant change after the long-term durability measurement (Fig. S9†), which also proves the good OER durability in alkaline electrolyte. To investigate the changes in structure and morphology post OER, Cu_3P NWs/CF after 22 h chronoamperometry test in 1.0 M KOH solution was characterized by SEM, TEM, and XPS. SEM and TEM images show that the nanowires morphology of the Cu_3P NWs/CF electrode was maintained post-OER test (Fig. S10†). Comparing to initial Cu_3P NWs/CF, the XPS spectrum of Cu 2p in Cu_3P NWs/CF after OER test showed two additional peaks at 933.5 eV (Cu $2p_{3/2}$) and 953.4 eV (Cu $2p_{1/2}$), which can be ascribed to the Cu^{2+} species (Fig. S11a†).[51] This surface electrochemical oxidation process was also confirmed by the P 2p XPS spectrum (Fig. S11b†).[52] Meanwhile, such an electrochemical oxidative transformation has been reported for other phosphatides-based OER electrocatalysts under alkaline electrolyte.[53] Similar to the previous reported electrocatalysts,[54,55] it is considered that the *in situ* formed phosphate layer is promoting the proton-coupled electron transfer process *via* unstable high valence Cu–oxo intermediate for enhancing OER activity.[56–60]

In order to further obtain the OER working electrode meeting the requirements of practical application, this simple two-step strategy was used to prepare a large-area electrode (40 cm^{-2}). As shown in Fig. 6a, the surface of the whole Cu foam is completely covered by $Cu(OH)_2$ after electrodeposition. After further low-temperature phosphating, a black Cu_3P electrode was obtained (Fig. 6b). The edge and central regions of $Cu(OH)_2$ and Cu_3P were characterized by SEM. As shown in Fig. 6c1-3 and d1-3, both $Cu(OH)_2$ and Cu_3P show uniform nanowire morphology, which indicates that this simple two-step method can be used for large-area preparation of OER electrode. XRD patterns (Fig. 6e and f) further confirmed that the large-area of $Cu(OH)_2$ and Cu_3P nanowires were successfully synthesized. Finally, the OER catalytic activity and stability of the large-area Cu_3P electrode was tested.

After about 100 CV cycles of activation, the large-area Cu_3P electrode was measured by chronoamperometry for 40 hours. As shown in Fig. 6g, after 40 hours of continuous OER reaction, Cu_3P electrode can operate stably at a current density of 10 mA cm^{-2}. Even at high current density of 100 mA cm^{-2}, no obvious attenuation of current density was observed, and the nanowire structure can still be maintained after stability measurement.

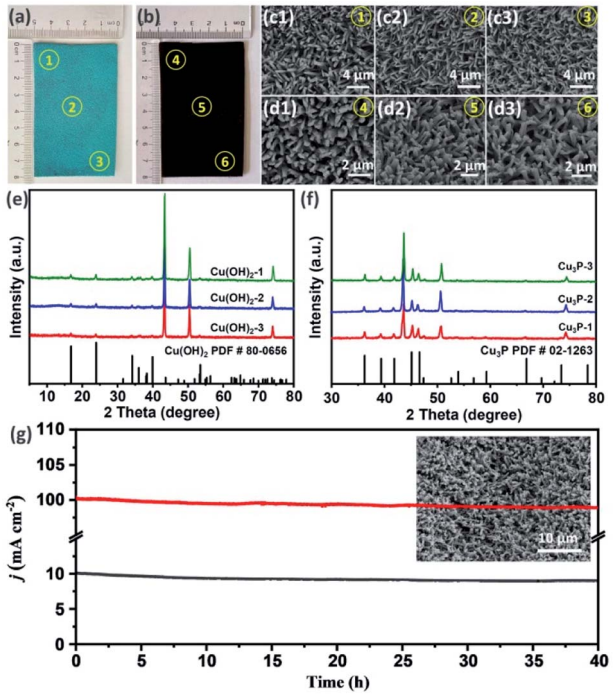

Fig. 6 Large-area (40 cm^{-2}) optical photograph of (a) $Cu(OH)_2$ NWs/CF and (b) Cu_3P NWs/CF. (c1-3) SEM images of regions 1, 2, and 3 in figure (a). (d1-3) SEM images of regions 4, 5, and 6 in figure (b). (e) XRD patterns of regions 1, 2, and 3 in figure (a). (f) XRD patterns of regions 4, 5, and 6 in figure (b). (g) Long-term stability of Cu_3P NWs/CF at 10 mA cm^{-2} (1.55 V) and 100 mA cm^{-2} (1.63 V) (inset is the SEM image of Cu_3P NWs/CF after long-term durability measurement at 100 mA cm^{-2}).

Conclusions

In summary, we demonstrate the preparation of self-supported Cu_3P nanowires on Cu foam (Cu_3P NWs/CF) and their application for high-efficiency electrocatalytic OER. $Cu(OH)_2$ nanowires were *in situ* grown on Cu foam ($Cu(OH)_2$ NWs/CF) by electrochemical of anodic oxidation in this paper, which is facilely converted into Cu_3P nanowires with a low temperature phosphorization process under N_2 atmosphere. The resulting Cu_3P NWs/CF exhibits enhanced activity toward OER with a small overpotential of 327 mV at the current density of 20 mA cm^{-2}, and good durability in alkaline medium. The unique nanowire structure, high conductivity of the electrocatalyst, and the reduced interfacial gap can effectively reduce the resistance of charge transfer as well as provide a large number of available active sites, thus enhancing the OER performance. More importantly, this simple two-step strategy is facile to fabricate large-area electrodes with uniform nanowire structure, which may promote future development of other catalysts in large-scale for water electrolysis.

Conflicts of interest

There are no conflicts to declare.

Acknowledgements

Funding for this work was received from the National Natural Science Foundation of China with the granted numbers of 21875056 and 22075231 and from Sichuan Science and Technology Program with the granted numbers of 2020YFSY0026 and 2021YFSY0022, for which the authors are greatly

appreciative. Limin Liu gratefully acknowledges the financial support of the Fundamental Research Funds for the Central Universities (2572018BC29), and the National Natural Science Foundation of Heilongjiang Province (B2018002).

Notes and references

1 N.-T. Suen, S.-F. Hung, Q. Quan, N. Zhang, Y.-J. Xu and H. M. Chen, *Chem. Soc. Rev.*, 2017, **46**, 337–365.
2 L. M. Gandía, R. Oroz, A. Ursúa, P. Sanchis and P. M. Diéguez, *Energy Fuels*, 2007, **21**, 1699–1706.
3 E. Hu, Y. Feng, J. Nai, D. Zhao, Y. Hu and X. W. D. Lou, *Energy Environ. Sci.*, 2018, **11**, 872–880.
4 L. Yan, L. Cao, P. Dai, X. Gu, D. Liu, L. Li, Y. Wang and X. Zhao, *Adv. Funct. Mater.*, 2017, **27**, 1703455.
5 H. Jiang, J. Gu, X. Zheng, M. Liu, X. Qiu, L. Wang, W. Li, Z. Chen, X. Ji and J. Li, *Energy Environ. Sci.*, 2019, **12**, 322–333.
6 K. Zhu, X. Zhu and W. Yang, *Angew. Chem., Int. Ed.*, 2019, **58**, 1252–1265.
7 Y. Guo, P. Yuan, J. Zhang, H. Xia, F. Cheng, M. Zhou, J. Li, Y. Qiao, S. Mu and Q. Xu, *Adv. Funct. Mater.*, 2018, **28**, 1805641.
8 K. A. Stoerzinger, O. Diaz-Morales, M. Kolb, R. R. Rao, R. Frydendal, L. Qiao, X. R. Wang, N. B. Halck, J. Rossmeisl and H. A. Hansen, *ACS Energy Lett.*, 2017, **2**, 876–881.
9 Y.-H. Fang and Z.-P. Liu, *J. Am. Chem. Soc.*, 2010, **132**, 18214–18222.
10 Y. Lee, J. Suntivich, K. J. May, E. E. Perry and Y. Shao-Horn, *J. Phys. Chem. Lett.*, 2012, **3**, 399–404.
11 A. Parra-Puerto, K. L. Ng, K. Fahy, A. E. Goode, M. P. Ryan and A. Kucernak, *ACS Catal.*, 2019, **9**, 11515–11529.
12 C. G. Read, J. F. Callejas, C. F. Holder and R. E. Schaak, *ACS Appl. Mater. Interfaces*, 2016, **8**, 12798–12803.
13 K. Liu, F. Wang, P. He, T. A. Shifa, Z. Wang, Z. Cheng, X. Zhan and J. He, *Adv. Energy Mater.*, 2018, **8**, 1703290.
14 H. Liu, J. Guan, S. Yang, Y. Yu, R. Shao, Z. Zhang, M. Dou, F. Wang and Q. Xu, *Adv. Mater.*, 2020, 2003649.
15 Y. Lin, L. Yang, Y. Zhang, H. Jiang, Z. Xiao, C. Wu, G. Zhang, J. Jiang and L. Song, *Adv. Energy Mater.*, 2018, **8**, 1703623.
16 L.-A. Stern, L. Feng, F. Song and X. Hu, *Energy Environ. Sci.*, 2015, **8**, 2347–2351.
17 Y. Yao, N. Mahmood, L. Pan, G. Shen, R. Zhang, R. Gao, F.-e. Aleem, X. Yuan, X. Zhang and J.-J. Zou, *Nanoscale*, 2018, **10**, 21327–21334.
18 M. B. Stevens, L. J. Enman, A. S. Batchellor, M. R. Cosby, A. E. Vise, C. D. Trang and S. W. Boettcher, *Chem. Mater.*, 2017, **29**, 120–140.
19 R. Xu, R. Wu, Y. Shi, J. Zhang and B. Zhang, *Nano Energy*, 2016, **24**, 103–110.
20 T. Wu, M. Pi, D. Zhang and S. Chen, *J. Mater. Chem. A*, 2016, **4**, 14539–14544.
21 T. Y. Ma, S. Dai, M. Jaroniec and S. Z. Qiao, *J. Am. Chem. Soc.*, 2014, **136**, 13925–13931.
22 N. Jiang, B. You, M. Sheng and Y. Sun, *Angew. Chem., Int. Ed.*, 2015, **127**, 6349–6352.
23 J. Song, C. Wei, Z.-F. Huang, C. Liu, L. Zeng, X. Wang and Z. J. Xu, *Chem. Soc. Rev.*, 2020, **49**, 2196–2214.
24 J. Du, F. Li and L. Sun, *Chem. Soc. Rev.*, 2021, **50**, 2663–2695.
25 P. Zhang, L. Li, D. Nordlund, H. Chen, L. Fan, B. Zhang, X. Sheng, Q. Daniel and L. Sun, *Nat. Commun.*, 2018, **9**, 1–10.
26 C.-C. Hou, Q.-Q. Chen, C.-J. Wang, F. Liang, Z. Lin, W.-F. Fu and Y. Chen, *ACS Appl. Mater. Interfaces*, 2016, **8**, 23037–23048.
27 A. Han, H. Zhang, R. Yuan, H. Ji and P. Du, *ACS Appl. Mater. Interfaces*, 2017, **9**, 2240–2248.
28 J. Xia, H. Zhao, B. Huang, L. Xu, M. Luo, J. Wang, F. Luo, Y. Du and C. H. Yan, *Adv. Funct. Mater.*, 2020, **30**, 1908367.
29 X. Zhou, W. Qi, K. Yin, N. Zhang, S. Gong, Z. Li and Y. Li, *Front. Chem.*, 2020, **7**, 900.
30 W. Jiang, J. Chen, G. Qian, H. He, H. Zhang, X. Zhuo, F. Shen, L. Luo and S. Yin, *Electrochim. Acta*, 2021, **390**, 138887.
31 J. Liu, G. Qian, H. Zhang, J. Chen, Y. Wang, H. He, L. Luo and S. Yin, *Chem. Eng. J.*, 2021, **426**, 131253.
32 J. Chen, Y. Wang, G. Qian, T. Yu, Z. Wang, L. Luo, F. Shen and S. Yin, *Chem. Eng. J.*, 2021, **421**, 129892.
33 G. Qian, J. Chen, T. Yu, L. Luo and S. Yin, *Micro Nano Lett.*, 2021, **13**, 1–13.
34 Y. Wang, G. Qian, Q. Xu, H. Zhang, F. Shen, L. Luo and S. Yin, *Appl. Catal., B*, 2021, **286**, 119881.
35 F. Shen, Y. Wang, G. Qian, W. Chen, W. Jiang, L. Luo and S. Yin, *Appl. Catal., B*, 2020, **278**, 119327.
36 Q. Wang, Z. Zhang, C. Cai, M. Wang, Z. L. Zhao, M. Li, X. Huang, S. Han, H. Zhou, Z. Feng, L. Li, J. Li, H. Xu, J. S. Francisco and M. Gu, *J. Am. Chem. Soc.*, 2021, **143**, 13605–13615.
37 J. Tian, Q. Liu, N. Cheng, A. M. Asiri and X. Sun, *Angew. Chem., Int. Ed.*, 2014, **126**, 9731–9735.
38 H. Pfeiffer, F. Tancret and T. Brousse, *Electrochim. Acta*, 2005, **50**, 4763–4770.
39 M. Kong, H. Song and J. Zhou, *Adv. Energy Mater.*, 2018, **8**, 1801489.
40 J. Li, G. Wei, Y. Zhu, Y. Xi, X. Pan, Y. Ji, I. V. Zatovsky and W. Han, *J. Mater. Chem. A*, 2017, **5**, 14828–14837.
41 C. Du, L. Yang, F. Yang, G. Cheng and W. Luo, *ACS Catal.*, 2017, **7**, 4131–4137.
42 T. Wang, H. Chen, Z. Yang, J. Liang and S. Dai, *J. Am. Chem. Soc.*, 2020, **142**, 4550–4554.
43 A. Wu, Y. Xie, H. Ma, C. Tian, Y. Gu, H. Yan, X. Zhang, G. Yang and H. Fu, *Nano Energy*, 2018, **44**, 353–363.
44 J. Chen, F. Zheng, S.-J. Zhang, A. Fisher, Y. Zhou, Z. Wang, Y. Li, B.-B. Xu, J.-T. Li and S.-G. Sun, *ACS Catal.*, 2018, **8**, 11342–11351.
45 D. Chen, J. Zhu, X. Mu, R. Cheng, W. Li, S. Liu, Z. Pu, C. Lin and S. Mu, *Appl. Catal., B*, 2020, **268**, 118729.
46 S. L. Zhang, B. Y. Guan, X. F. Lu, S. Xi, Y. Du and X. W. Lou, *Adv. Mater.*, 2020, **32**, 2002235.
47 L. Zhang, L. Wang, Y. Wen, F. Ni, B. Zhang and H. Peng, *Adv. Mater.*, 2020, **32**, 2002297.
48 H. Zhang, A. W. Maijenburg, X. Li, S. L. Schweizer and R. B. Wehrspohn, *Adv. Funct. Mater.*, 2020, 2003261.
49 Y. Li, Z. Wang, J. Hu, S. Li, Y. Du, X. Han and P. Xu, *Adv. Funct. Mater.*, 2020, 1910498.

50 C. Liang, P. Zou, A. Nairan, Y. Zhang, J. Liu, K. Liu, S. Hu, F. Kang, H. J. Fan and C. Yang, *Energy Environ. Sci.*, 2020, **13**, 86–95.
51 Z. Hu, Q. Liu, W. Lai, Q. Gu, L. Li, M. Chen, W. Wang, S. L. Chou, Y. Liu and S. X. Dou, *Adv. Energy Mater.*, 2020, **10**, 1903542.
52 Q. Shi, Q. Liu, Y. Ma, Z. Fang, Z. Liang, G. Shao, B. Tang, W. Yang, L. Qin and X. Fang, *Adv. Energy Mater.*, 2020, **10**, 1903854.
53 Y. Hou, X. Zhuang and X. Feng, *Small Methods*, 2017, **1**, 1700090.
54 J. Lu, X. Luo, T. Wu, K. Amine and L. Ma, *Division of Fuel Chemistry Preprints*, American Chemical Society, 2016.
55 J. Lu, S. Yin and P. K. Shen, *Electrochem. Energy Rev.*, 2019, **2**, 105–127.
56 J. Xu, J. Li, D. Xiong, B. Zhang, Y. Liu, K.-H. Wu, I. Amorim, W. Li and L. Liu, *Chem. Sci.*, 2018, **9**, 3470–3476.
57 W. Li, D. Xiong, X. Gao and L. Liu, *Chem. Commun.*, 2019, **55**, 8744–8763.
58 F. Hu, S. Zhu, S. Chen, Y. Li, L. Ma, T. Wu, Y. Zhang, C. Wang, C. Liu and X. Yang, *Adv. Mater.*, 2017, **29**, 1606570.
59 R.-Q. Li, B.-L. Wang, T. Gao, R. Zhang, C. Xu, X. Jiang, J. Zeng, Y. Bando, P. Hu and Y. Li, *Nano Energy*, 2019, **58**, 870–876.
60 S. Riyajuddin, S. Tarik Aziz, S. Kumar, G. D. Nessim and K. Ghosh, *ChemCatChem*, 2020, **12**, 1394–1402.